

# Dynamics of ablation plumes produced by fusion products in laser fusion liquid wall chamber

Hiroyuki Furukawa  
*Institute for Laser Technology*

(Received: 25 August 2008 / Accepted: 17 November 2008)

An integrated ablation simulation code DECORE ( DESIGN COde for REactor ) has been developed to analyze characteristics of plumes produced by ablation, and to clarify the ability of the chamber clearance. Characteristics of a plume produced by ablation in liquid wall chamber of KOYO-fast have been analyzed. A plume produced by ablation moves with velocities of a few km/s. Formation of clusters in a plume with hydrodynamic motion is carried out. Radius of clusters in a plume in liquid wall chamber of KOYO-fast is mainly from 25 nm to 35 nm.

Keywords: simulation, chamber clearance, liquid wall, plume, ablation, cluster

## 1. Introduction

A design of laser fusion reactor with a liquid wall, KOYO-fast, is reported in Refs. 1-3. Fig. 1 shows the simple outline of the first wall of KOYO-fast.

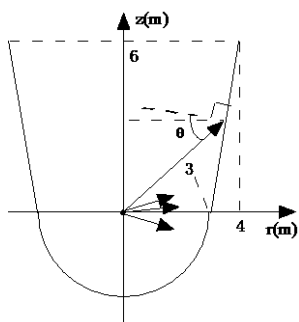


Fig. 1 The simple outline of the first wall of KOYO-fast.

One of the critical issue of a laser fusion reactor with a liquid wall is the chamber clearance. After micro explosion with 100 MJ nuclear yield, about 10 kg of liquid metal evaporates from the surface due to heating by  $\alpha$  particles, ions and debris from the target. Contribution of X-ray on the ablation is negligible in the case of direct implosion[4]. The evaporated plume makes, then, mist and clusters after expansion cooling. Such clusters would attach on the injected target surface and degrade the target performance through RT instabilities and preheat of the fuel. Fig 2 shows phenomena which occurs nearby first wall of KOYO-fast.

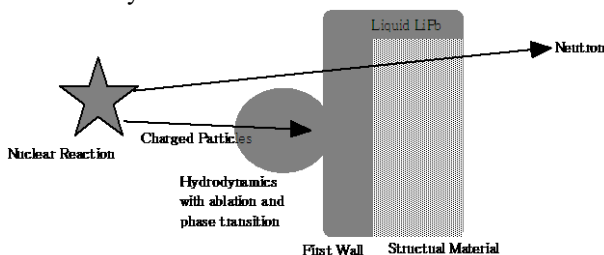


Fig 2 Phenomena which occurs nearby first wall of KOYO-fast.

To experimentally simulate the ablation process, laser irradiation is often used. I, however, found that ablation process by ions is quite different from that by lasers. The range of  $\alpha$  particles in liquid Pb is about 10  $\mu$ m. As the result, superficial liquid Pb evaporates as a high density, low temperature, plasma with low ionization rate.

In this study, I have developed an integrated ablation simulation code DECORE ( Design Code for Reactor ) to clarify the ability of the chamber clearance. In this integrated simulation code, effects of condensation of a plume, phase transition from liquid to neutral gas to partially ionized plasma, absorption of energies of charged particles, equation of state, hydrodynamics, and radiation transport are included. I estimate temperatures, densities, and velocities and so on of ablated lead ( liquid wall material ) using DECORE for the case of first ignition with 200 MJ power output[5].

A new model on stopping power in high Z and low temperature plasmas has been developed in this study. Electrons in metal consists of conduction electrons, resonance electrons, and bound electrons. Resonance electrons behave like free electrons due to physical phenomena. Resonance electrons are obtained by functions of binding energy, population, and energy of incident charged particles.

In an integrated simulation code 'DECORE', the formation of clusters in the ablated plume in a laser fusion reactor is evaluated by a new model based on Luk'yanchuk-Zeldovich-Raizer model[6]. Luk'yanchuk-Zeldovich-Raizer model is described for the case of spherically symmetric and adiabatic expansion. A new model is written for arbitrary profiles.

Characteristics of a plume produced by ablation in liquid wall chamber of KOYO-fast have been analyzed. Due to the design of KOYO-fast, the shortest length from

a pellet to wall of a chamber is 3 m. A plume produced by ablation moves with velocities of a few km/s. Formation of clusters in a plume with hydrodynamic motion is carried out. Radius of clusters in a plume in liquid wall chamber of KOYO-fast is mainly from 25 nm to 35 nm.

In section 2, basic equations of DECORE are described. In section 3, I summarize simulation results and discuss.

## 2. Basic Equations of DECORE

### 2.1 Schematic Diagram of DECORE

Fig. 3 shows the schematic diagram of DECORE. First, by using of atomic process code, data of ionization degree, population and energy levels are obtained. Second, using these data, stopping power, equation of state, emissivity and opacity data are obtained. Finally, using these data, hydrodynamic simulations with phase transitions, ablation, radiation transport, and so on, are performed.

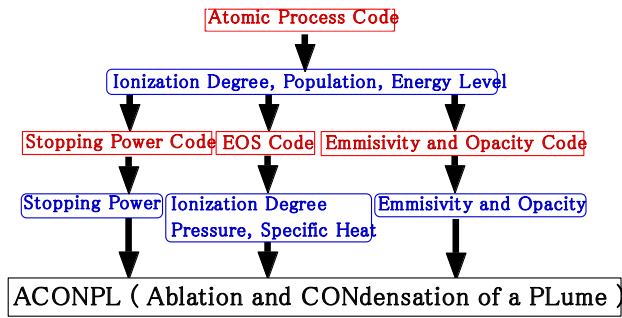


Fig. 3 The schematic diagram of DECORE.

### 2.2 Main Program of DECORE

Main program of DECORE consists of energy absorptions of external X-rays and charged particles, phase transitions from liquid to gas to plasma, condensation of a plume, ablation process, hydrodynamics, radiation transport of X-ray. In this paper, this program is named ‘ACONPL (Ablation and CONDensation of a PLume)’. Fig. 4 is flow chart of ACONPL.

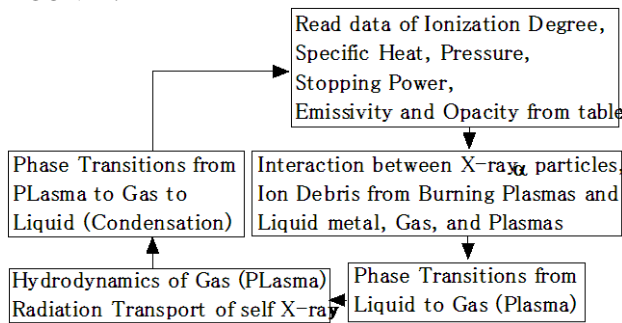


Fig. 4 Flow chart of ACONPL.

### 2.2.1 Equation of Motion on the Ablation Surface

Ablation surface  $x_v(t)$  moves according to eq. 1 [7].

$$\frac{\partial}{\partial t} x_v(t) = \sqrt{k_B T_v / m_i} \cdot \exp(-m_i L_v / k_B T_v) \quad (1)$$

where  $k_B$  is Boltzmann constant,  $L_v$  is latent heat of vaporization,  $m_i$  is mass of atom, and

$$T_v = T_i(x) \quad (2)$$

### 2.2.2 Equation of Energy Density in Liquid ; $U_l$

Energy density in liquid,  $U_l$  is given as follows.

$$\frac{\partial U_l}{\partial t} = \nabla \cdot [\kappa_l \nabla T_l(x, t)] + Q_p(x, t) + Q_X(x, t) + Q_{rad}(x, t) \quad x_v < x < x_{max} \quad (3)$$

$$U_l(x, t) \equiv \rho_l \left\{ \int_{T_0}^{T_l(x, t)} C_l(x, T_l(x, t)) dT + \Delta_l(x, t) \right\} \quad (4)$$

Where  $\kappa_l$  the thermal conductivity of liquid,  $Q_p$  the heat quantity due to external charged particles,  $Q_X$  the heat quantity due to external X-ray,  $Q_{rad}$  the heat quantity due to self X-ray,  $C_l$  the specific heat of liquid,  $\rho_l$  is the mass density of liquid, and  $\Delta_l$  is internal energy of liquid.

Boundary condition of equation of thermal conduction is as follows.

$$\left. \frac{\kappa_l}{\rho_l} \frac{\partial T_l(x, t)}{\partial t} \right|_{x=x_v} = L_v \frac{\partial}{\partial t} x_v(t) \quad (5)$$

The critical value of  $U$ , namely  $U^{crit}$  is determined as follows.

$$U_l^{crit} = \rho_l \left\{ \int_{T_0}^{T_{vap}} C_l(x, T) dT + L_v \right\} \quad (6)$$

Where  $T_{vap}$  is vaporization temperature, and  $T_0$  is initial temperature.

If  $U > U^{crit}$ , peeling will occur.

### 2.2.3 Fluid Equation of Gas and Partially Ionized Plasma

Ablated materials behave according to fluid equations ( 1 fluid and 2 temperature Lagrange scheme model ).

$$\frac{d\rho(x, t)}{dt} = -\rho(x, t) \nabla \cdot v(x, t) \quad (7)$$

$$\rho(x, t) \frac{dv(x, t)}{dt} = -\nabla [P_e(x, t) + P_i(x, t) + P_{nv}(x, t)] \quad (8)$$

$$\begin{aligned} \rho(x, t) c_v^{(e)} \frac{dT_e(x, t)}{dt} &= -\nabla \cdot q_e(x, t) \\ &- \gamma [T_e(x, t) - T_i(x, t)] - P_{ih}^{(e)}(x, t) \nabla \cdot v(x, t) \\ &+ Q_p(x, t) + Q_X(x, t) + Q_{rad}(x, t) \end{aligned} \quad (9)$$

$$\begin{aligned} \rho(x,t)c_v^{(i)} \frac{dT_i(x,t)}{dt} = & -\nabla \cdot q_i(x,t) \\ & + \gamma [T_e(x,t) - T_i(x,t)] \\ & - [P_{th}^{(i)}(x,t) + P_{nv}(x,t)] \nabla \cdot v(x,t) \\ & + \rho(x,t)c_v^{(i)} \left[ \frac{2}{3}q - T(x,t) \right] \left( \frac{\alpha}{\theta} \right)^3 \frac{dv(x,t)}{dt} \end{aligned} \quad (10)$$

Where,  $T_e$  is electron temperature,  $T_i$  is ion temperature,  $\gamma$  is energy relaxation constant from electron to ion.  $v(x,t)$  is the rate of nucleation described in next section.

Specific heat  $c_v^{(s)}$  and pressure  $P_s$  are given by equation of state.  $P_{nv}$  is numerical viscosity[8].  $P_{th}^{(s)}$  is defined as follows.

$$P_{th}^{(s)}(x,t) = T_s(x,t) \left[ \frac{\partial P^{(s)}(x,t)}{\partial T_s} \right]_\rho \quad (11)$$

4-th term of right hand side of eq. (10) stands energy production due to condensation of a plume described in next section.

#### 2.2.4 Condensation of a Plume[6, 9, 10]

Condensation temperature  $T_c(\rho)$ , which depends on mass density, is introduced as follows.

$$T_c(\rho) = q \Phi(\rho) \quad (12)$$

Where  $q$  is the latent heat of vaporization given in Kelvin,  $\Phi(\rho)$  is the smaller root of the transcendental equation.

$$\frac{1}{\Phi(\rho)^3} \exp \left[ -\frac{1}{\Phi(\rho)} \right] = \frac{R_g T_s}{\mu P_s} \rho \left( \frac{q^2}{T_s T_\ell} \right)^{3/2} \quad (13)$$

Where  $T_s = 300$  K,  $R_g$  is the gas constant,  $\mu$  is atomic weight of the vapor,  $P_s$  is the pre-exponential factor in the equation for saturated vapor pressure.

The degree of condensation is given as follows.

$$y(x,t) = v(x,t) \cdot g(x,t) \quad (14)$$

The rate of nucleation  $v(x,t)$  is given as follows.

$$\begin{aligned} \frac{dv(x,t)}{dt} = & 4 \frac{\rho(x,t)}{\rho_\ell} \sqrt{\frac{2\sigma}{\pi m_i}} [1 - y(x,t)] \\ & \times \exp \left[ -\frac{T_{nuc}}{T(x,t)} \frac{1}{\theta(x,t)^2} \right] \end{aligned} \quad (15)$$

$$T_{nuc} = \frac{16\pi\sigma^3 m_i^2}{3k_B^3 q^2 \rho_\ell^2} \quad (16)$$

Where  $\rho_\ell$  is mass density of liquid,  $\sigma$  is surface tension,  $m_i$  is mass of atom of vapor, and  $\theta$  is super cooling parameter defined as

$$\theta(x,t) = \frac{T_i(x,t) - T(x,t)}{T_i(x,t)} \quad (17)$$

Where  $T(x,t)$  is temperature of cluster obtained by solving eq. (20).

The equation for cluster growth can be written as follows.

$$\begin{aligned} \frac{dg(x,t)}{dt} = & \frac{\pi \rho(x,t)}{m_i} \left( \frac{3m_i}{4\pi \rho_\ell} \right)^{2/3} \sqrt{\frac{8k_B}{\pi m_i}} g^{2/3} \sqrt{T} \\ & \times [1 - y(x,t)] \left\{ 1 - \exp \left[ -\frac{q}{T} (\theta - \alpha g^{-1/3}) \right] \right\} \end{aligned} \quad (18)$$

$$\alpha = \frac{2\sigma m_i}{k_B q \rho_\ell} \left( \frac{4\pi \rho_\ell}{3m_i} \right)^{1/3} \quad (19)$$

Here,  $g$  is defined as the number of atoms gathering to a nucleation center.

Temperature of cluster  $T(x,t)$  is obtained by solving following equation.

$$\begin{aligned} [1 + y(x,t)] \frac{dT(x,t)}{dt} \\ + [1 - y(x,t)] \frac{2T(x,t)}{3} \left[ -\frac{1}{\rho(x,t)} \frac{d\rho(x,t)}{dt} \right] \\ = \left[ \frac{2}{3}q - T(x,t) \right] \frac{dy(x,t)}{dt} \end{aligned} \quad (20)$$

#### 2.2.5 Radiation Transport

Radiation transports are treated by flux-limited multi group diffusion approximation.

$$\begin{aligned} \rho(x,t) \left( \frac{E_v(x,t)}{\rho(x,t)} \right) = & - (F_v(x,t) - vE_v(x,t)) \\ & + 4\pi j(v, x, t) - c\kappa(v, x, t) E_v(x,t) \end{aligned} \quad (21)$$

$$F_v(x,t) = -\frac{c}{\frac{|\partial E_v(x,t)/\partial x|}{E_v(x,t)} + 3\kappa(v, x, t)} \frac{\partial E_v(x,t)}{\partial x} \quad (22)$$

where  $E_v$  is radiation energy density, and  $F_v$  is radiation flux.  $j(v)$  is emissivity, and  $\kappa(v)$  is opacity, and  $c$  is speed of light.

Heat quantity due to self emitted X-ray  $Q_{rad}$  is defined as follows.

$$Q_{rad}(x,t) = - \int dv [4\pi j(v, x, t) - c\kappa(v, x, t) E_v(x,t)] \quad (23) \quad (19)$$

#### 2.3 Stopping Power in High Z and Low Temperature Plasmas

A new model on stopping power in high  $Z$  and low temperature plasmas has been developed in this study. Stopping power due to free electrons is obtained by dielectric functions[11], and stopping power due to bound electrons is obtained by binary-encounter model[12]. Resonance electrons behave like free electrons due to

physical phenomena. Resonance electrons are obtained by functions of binding energy, population, and energy of incident charged particles.

Stopping power due to free electrons is described as follows.

$$W_{free}(E_k(x,t), \rho(x,t), T(x,t)) = \frac{4\pi n_{fe} Z_0^2 e^4}{m_e v^2} L_f \quad (24)$$

$$L_f = -\frac{1}{(2\pi)^3} \frac{m_e v}{n_{fe} e^2} \int d\mathbf{k} \frac{\mathbf{k} \cdot \mathbf{v}}{k^2} \text{Im} \frac{1}{\varepsilon(\mathbf{k}, \mathbf{k} \cdot \mathbf{v})} \quad (25)$$

Where  $Z_0 e$  is the charge of incident charged particles, and  $\varepsilon$  is dielectric function which consists of ion part and free electron, which includes resonance electron, part.  $n_{fe}$  is the number density of free electrons,  $m_e$  is mass of an electron

Stopping power due to bound electrons is described as follows.

$$W_{bound} = n_i \sum_n \sum_l I_{nl} P_{nl} \pi \left( \frac{Z_0 e^2}{I_{nl}} \right)^2 G \left( \frac{v}{v_{nl}} \right) \quad (26)$$

$$G(V) = 4V^4 / 15 \quad (V < 0.206) \quad (27)$$

$$G(V) = \frac{\alpha^{3/2}}{V^2} \left[ \alpha + \frac{2}{3} (1 + \beta) \ln(2.7 + V) \right] \quad (28)$$

$$(V > 0.206)$$

$$v_{n,l} = \sqrt{2I_{n,l} / m_e} \quad (29)$$

Where  $I_{nl}$  is binding energy of average atom model, and  $P_{nl}$  is the population of principal quantum number  $n$  and azimuthal quantum number  $l$  of average atom model.

Fig. 5 shows stopping power of  $\alpha$  particles in solid lead as a function of particle energy. Results of Ziegler model[13] and present model are in good agreement.

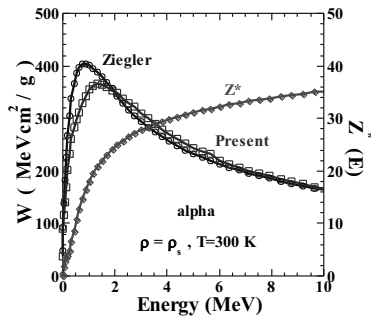


Fig. 5 Stopping power of  $\alpha$  particles in solid lead as a function of particle energy.

Fig. 6 shows heat quantity due to stopping power of  $\alpha$  particles in solid lead as a function of pass length. Note that initial energy of  $\alpha$  particle is 3.52 MeV. Both are in good agreement.

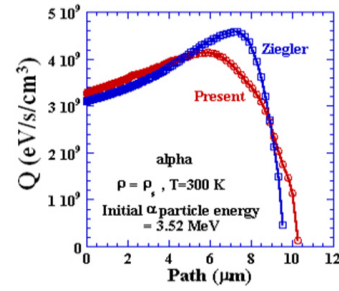


Fig. 6 Heat quantity due to stopping power of  $\alpha$  particles in solid lead as a function of pass length.

## 2.4 X-ray Spectra from Burning Plasmas and Absorption Coefficients

Fig. 7 shows X-ray spectra from burning plasmas[5] for the case using KOYO-fast target and laser system, and absorption coefficients as a function of energy of X-ray[14]. In previous work[15], I showed that heat quantity due to X-ray is very small because X-ray absorption coefficients of lead are very small at the photon energy of 10keV for the case of KOYO, direct ignition. Also in the case of KOYO-fast, heat quantity due to X-ray is very small because X-ray absorption coefficients of lead are very small at the photon energy of 10keV.

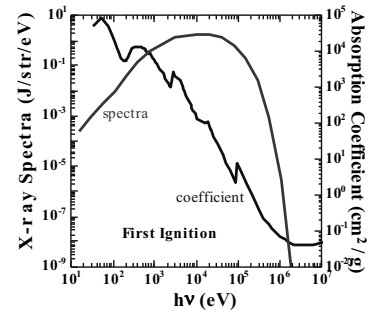


Fig. 7 X-ray spectra from burning plasmas for the case using KOYO-fast target and laser system, and absorption coefficients as a function of energy of X-ray.

## 2.5 Irradiated Intensity of Charged Particles on the Surface of Liquid Wall

Fig. 8 shows irradiated intensity of charged particles[5] on the surface of liquid wall at the distance of 3m from the target. Note that calculation in ref. 5 includes  $\alpha$ , deuterium, tritium, proton, and helium 3.

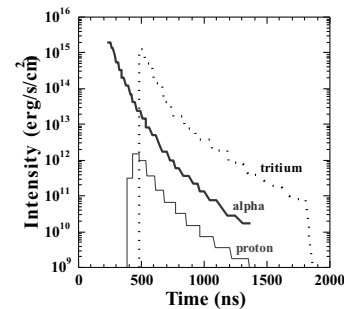


Fig. 8 Irradiated intensity of charged particles on the surface of liquid wall at the distance of 3m from the target.

### 3. RESULTS AND DISCUSSIONS

#### 3.1 Ablation Depth and Profiles of a Plume

I have estimated characteristics of a plume produced by ablation at a distance of 3 m from a target for the case of KOYO-fast. Fig. 9 shows ablation depth as a function of time. As Note that, when heating laser is irradiated on target, I set time = 0. As shown in Fig. 9, liquid lead with roughly 6  $\mu\text{m}$  thickness is peeled out suddenly. After peeling, almost of all energy of charged particles are absorbed by ablated materials. In the regime of liquid, only small energy of charged particles is reached.

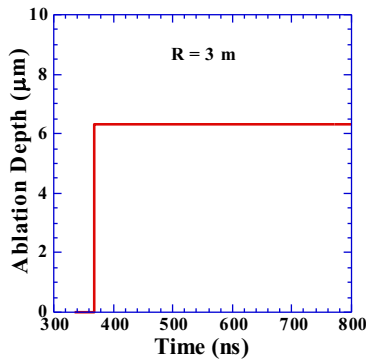


Fig. 9 Ablation depth as a function of time.

Fig. 10 shows number density and velocity profiles of lead. As shown in Fig. 10, ablated lead moves as a clump with velocities of a few km/s. To estimate this velocity is very important for analysis of protecting beam port from charged particles.

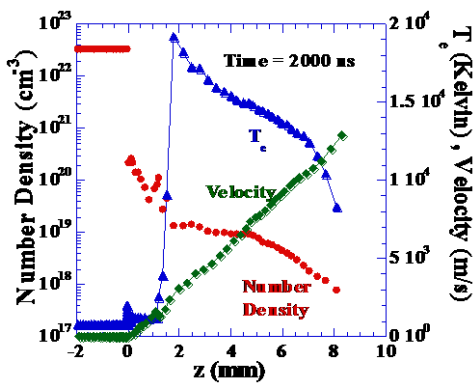


Fig. 10 Number density and velocity profiles of lead.

#### 3.2 Clusterization in a Plume

Fig. 11 shows profile of radius of clusters and condensation rate of a plume. This result is in good agreement with experimental results[16].

This subject is the first step to estimate collisions between plumes produced by ablation near the center of the liquid wall chamber. Collisions between plumes strongly affect a design of laser fusion reactor.

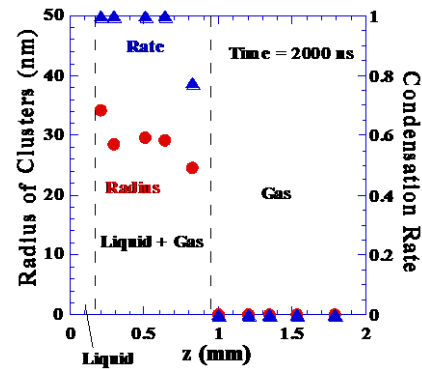


Fig. 11 Profile of radius of clusters and condensation rate of a plume.

### REFERENCES

- [1] Y. Kozaki, Fusion Science and Technology **49** (2006) 542-552.
- [2] Y. Kozaki et.al.; J. Plasma and Fusion Research **82** (2006) 817-837. (in Japanese)
- [3] Y. Kozaki et.al.; J. Plasma and Fusion Research **83** (2007) 3-29. (in Japanese)
- [4] H. Furukawa, Y. Kozaki, K. Yamamoto, T. Johzaki, and K. Mima ; Fusion Engineering and Design **73** (2005) 95-103.
- [5] T. Johzaki, K. Mima, Y. Nakao, H. Nagatomo, and A. Sunahara,; Proc. 3rd Inertial Fusion Sciences and Applications 2003.
- [6] B. S. Luk'yanchuk, W. Marine, S. I. Anisimov, and G. A. Simakina, SPIE **3618** (1999) 434-452.
- [7] S. I. Anisimov and V.A.Khoklov, "Instabilities in Laser- Matter Interaction", CRC Press (1995).
- [8] R. D. Richtmyer, and K. W. Morten, "Difference Method for Initial-Value Problems" (1967) Interscience Pub.
- [9] H. Furukawa, IFSA2007 Proceeding, IOP Publishing, Journal of Physics: Conference Series **112** (2008) 032041. <http://iopscience.iop.org/1742-6596/112/3/032041/>
- [10] H. Furukawa, to be published in Rev. Laser. Eng. Vol. 36, No. 11 (2008). (in Japanese)
- [11] H. Furukawa and K. Nishihara; Phys. Rev. A **46** (1992) 6596-6607.
- [12] T. Peter and J. Meyer-ter-Vehn, Phys. Rev. A **43** (1991) 2015-2029.
- [13] J. F. Ziegler, Stopping Cross-Sections for Energetic Ions in All Elements **5** (1980) 391.
- [14] Atomic data and Nuclear data Table **54** (1993) 181-342.
- [15] Hiroyuki Furukawa, Yasuji Kozaki, Keiji Yamamoto, Tomoyuki Johzaki, and Kunioki Mima, Fusion Engineering and Design **73** (2005) 95-103.
- [16] T. Ohshige, et. al.; IFSA2007 Proceeding, IOP Publishing, Journal of Physics: Conference Series **112** (2008) 032040. <http://iopscience.iop.org/1742-6596/112/3/032040/>